Supplemental Data

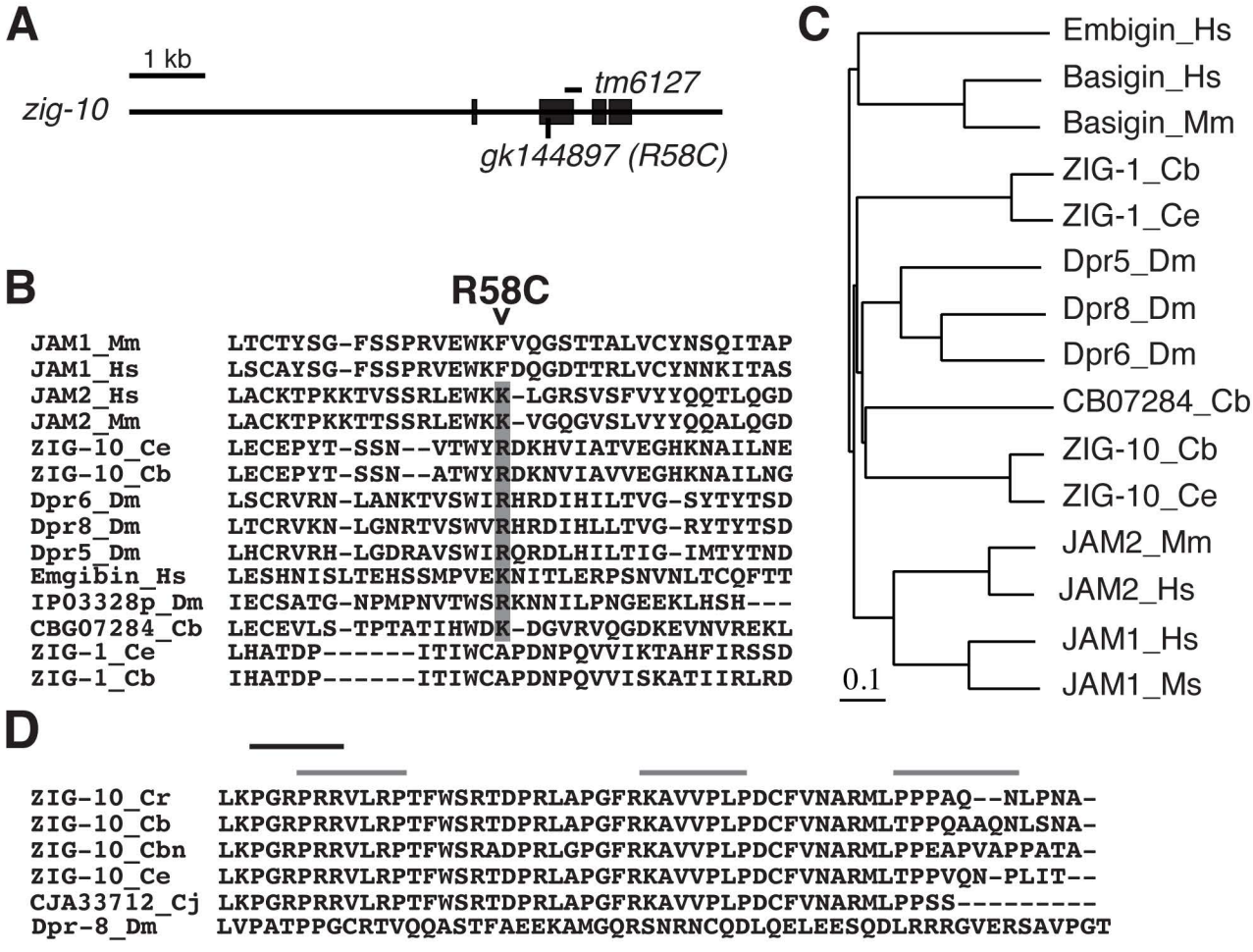

Figure S1, Related to Figure 1. Gene Structure and Homology of *zig-10*.

(A) The *zig-10* genomic locus is comprised of four exons and was cloned into pCZGY2602. The *tm6127* allele causes a 225bp deletion leading to a premature stop codon after amino acid 158 (see Table S3); the *gk144897* allele causes a C/t mutation, resulting in an R58C missense mutation.
(B) Homologs of ZIG-10 were identified as proteins that contain two Ig domains only followed by a transmembrane domain with no intracellular enzymatic domains using Simple Modular Architecture Research Tool (SMART) (Letunic et al., 2015). Proteins that contained additional domains were excluded from our analysis. Alignments of the first Ig domain of ZIG-10 homologs were generated using ClustalX2.1, and the R58C mutation occurs at a conserved residue.
(C) A phylogenetic tree of the two Ig domain-only transmembrane protein subfamily created using ClustalX2.1.
(D) An alignment of the intracellular domain of ZIG-10 homologs that contain SH3 ligand motifs. The black bar denotes the class II SH3 ligand motif; the gray bars indicate the three non-canonical SH3 ligand motifs. Cb = *C. briggsae*; Cbn = *C. brenneri*; Ce = *C. elegans*; Cj = *C. japonica*; Cr = *C. remanei*.

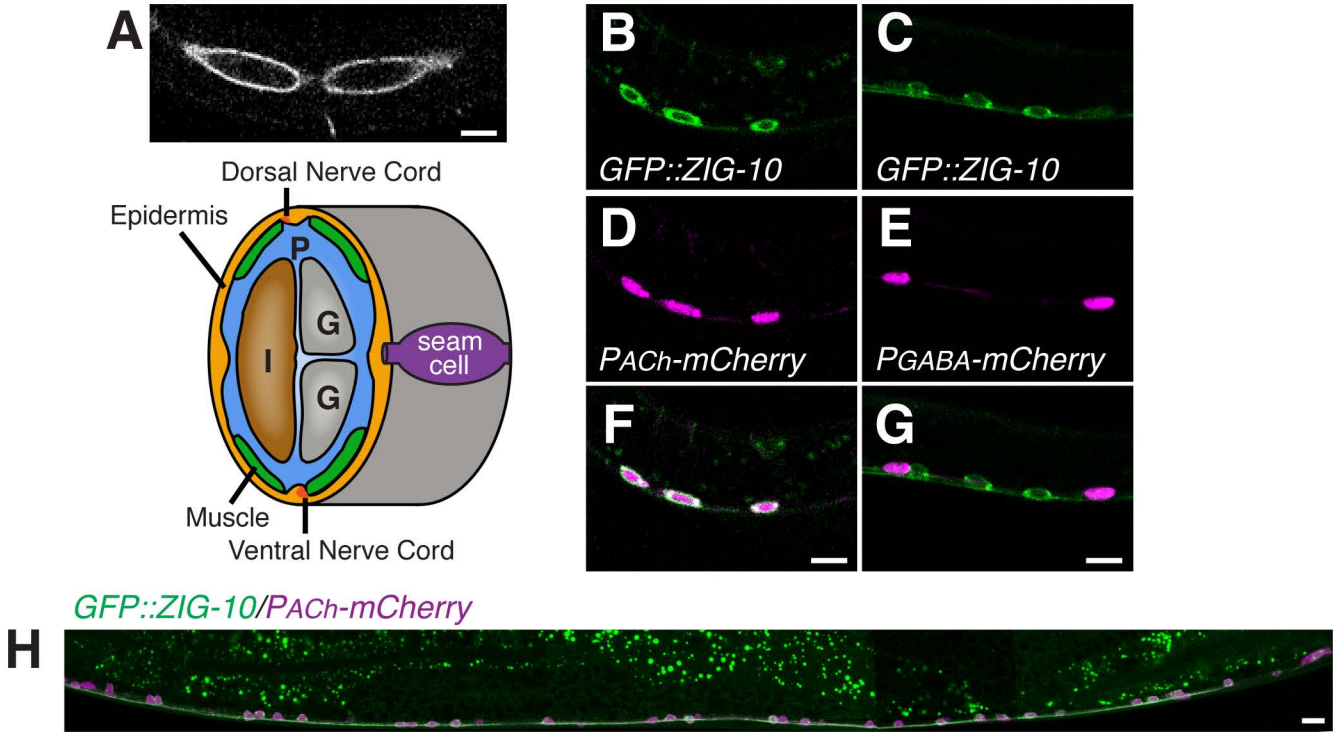

Figure S2, Related to Figure 2. ZIG-10 is Expressed in Epidermal cells and Cholinergic Motor Neurons.

(A) GFP::ZIG-10 expressed under the *zig-10* promoter (*juEx5455*) is visible at the junction between the epidermis and seam cells (upper panel). Diagram illustrating tissue location of seam cells (lower panel).Tissues are indicated as Intestine, I; Gonad, G; the Pseudocoelom is indicated as P. Scale bars, 5 μm.
(B-C) Ventral cord of L1 animals expressing GFP::ZIG-10 under the *zig-10* promoter *(juEx5455)*.
(D) P*unc-17β* driven mCherry in cholinergic neurons *(nuIs321)*.
(E) P*ttr-39* driven mCherry in GABAergic neurons *(juIs223)*.
(F-G) Merge of red and green channels. Scale bars, 5 μm.
(H) Montage of L4 animal expressing GFP::ZIG-10 (*juEx5455*) and Punc-17β-mCherry *(nuIs321)* in the ventral cord posterior to the retrovesicular ganglion. Scale bars are 10μm.

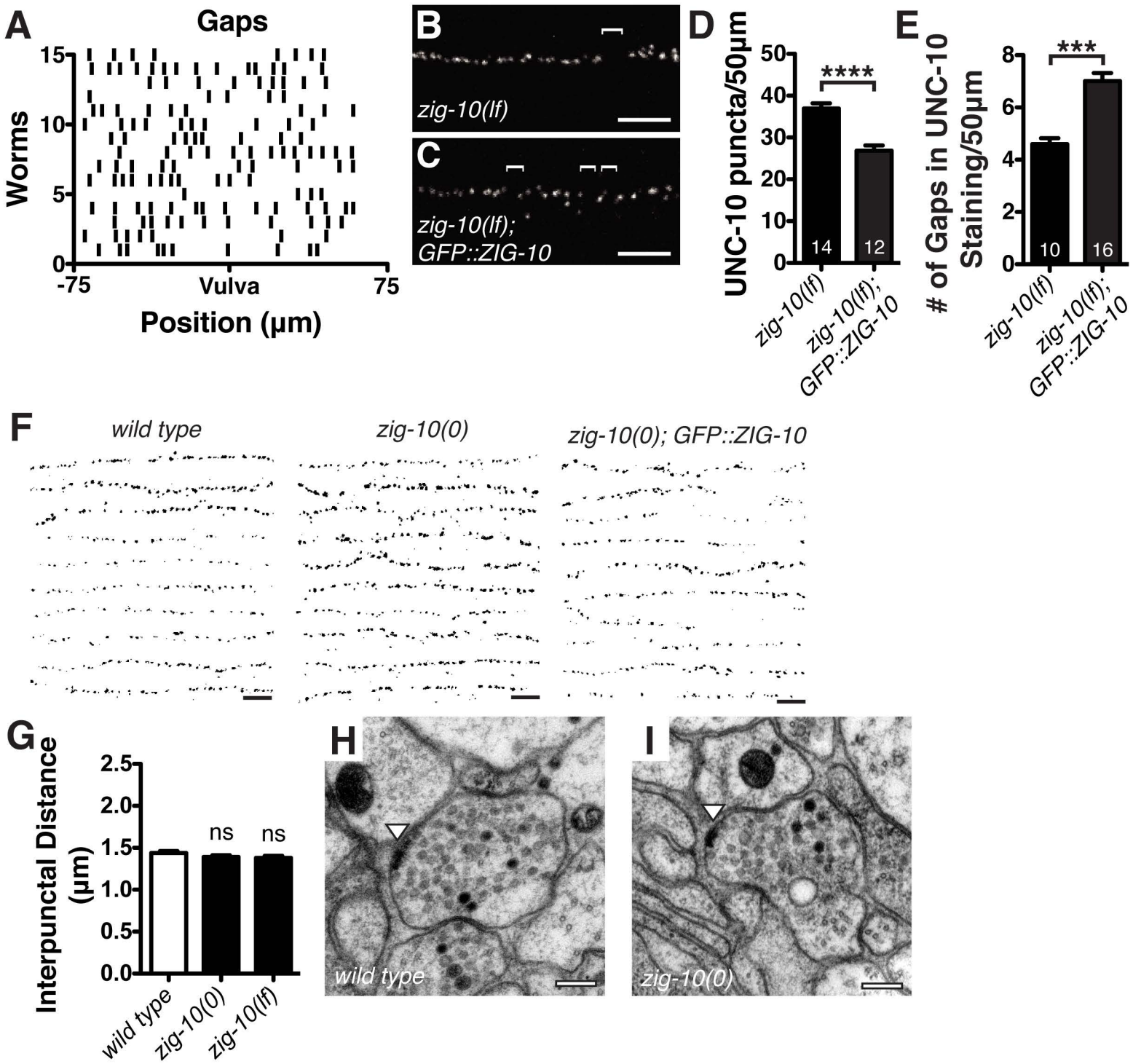

Figure S3, Related to Figure 3. zig-10 Alters Synapse Density, Not Neuron or Synapse Morphology.

(A) Synaptic gaps occur stochastically along the nerve cord. The vulva was used as a postional marker.
(B-C) Representative micrographs of UNC-10 staining in the dorsal nerve cord. Brackets indicate synaptic gaps. Scale bars, 5 µm.
(D) The increased density of UNC-10 puncta in zig-10(lf) animals is reduced by GFP::ZIG-10 expression.
(E) GFP::ZIG-10 expression increased the number of synaptic gaps in zig-10(lf) animals.
(F) Ten stacked representative micrographs converted to binary masks of UNC-10 staining in the dorsal nerve cord per genotype. Scale bars, 5 µm.
(G) The distance between adjacent synapses in not changed in *zig-10* mutants.
(H-I) Electron micrographs showing that synapse morphology is not altered in *zig-10(0)*. Arrowhead indicates dense projection of synapse. Scale bars, 200 nm.
The data in D, E, and G are are represented as mean ± SEM. ***p≤0.001, ****p≤0.0001, and ns=not significant.

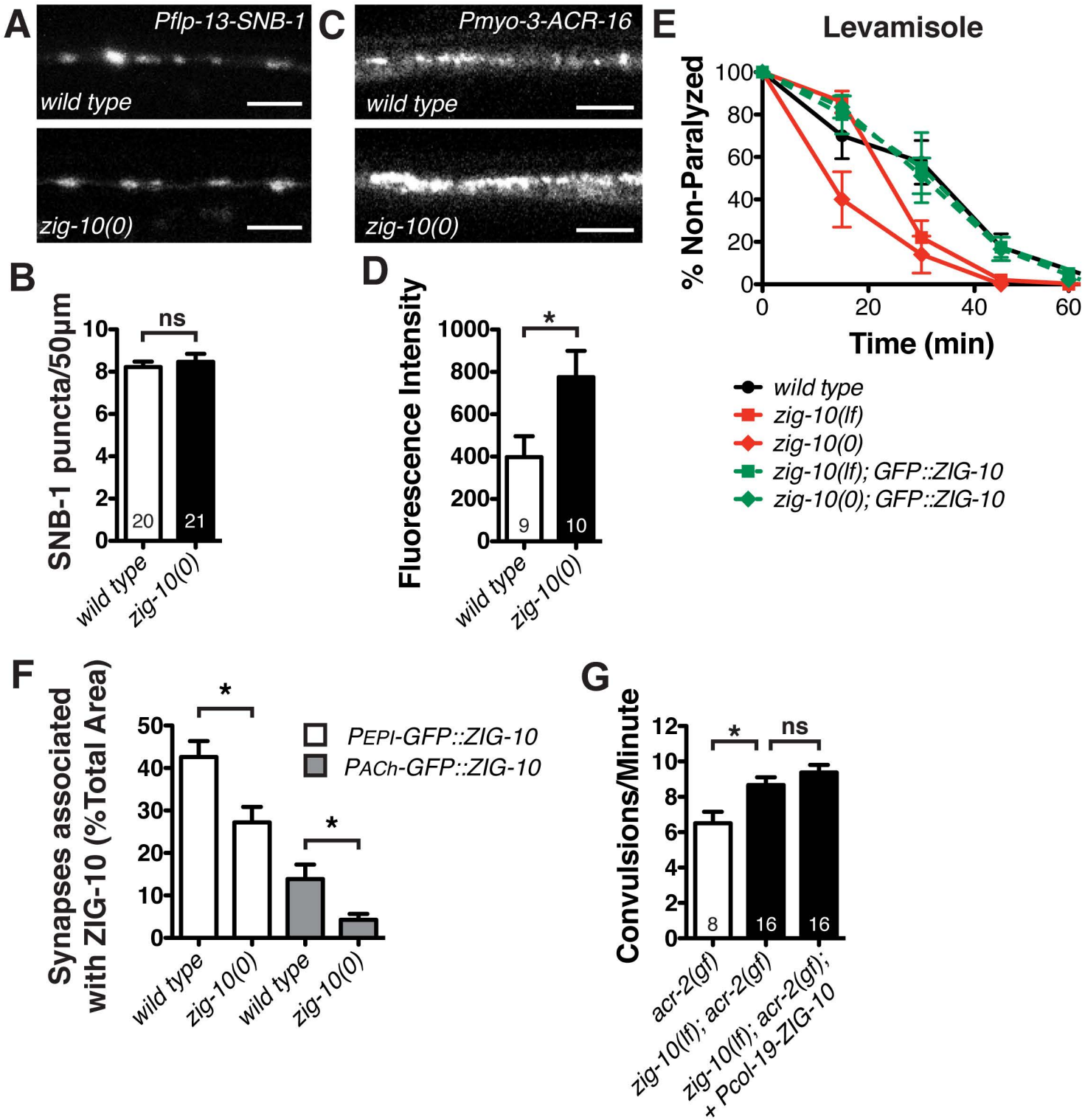

Figure S4, Related to Figure 4. *zig-10* Affects Cholinergic Synapses.

(A) Representative images of SNB-1::GFP *(juIs137)* expressed in GABAergic neurons.
(B) GABAergic synapses are normal in *zig-10(0)* animals.
(C) Representative images of ACR-16::GFP *(akIs46)* expression in dorsal muscle. Scale bars are 5 µm.
(D) *zig-10(0)* increased ACR-16::GFP intensity in arbitrary units as measured by integrated density (area x intensity).
(E) *zig-10* mutants are hypersensitive to 1 mM levamisole.
(F) The association of epidermal (*juEx5704*) or cholinergic (*juEx5706*) expression pattern of GFP::ZIG-10 with active zones stained for UNC-10 was analyzed. GFP staining within 1µm of a synapse was considered a postive association between ZIG-10 and synapses.
(G) Epidermal expression of ZIG-10 did not reduce the convulsion frequency in *zig-10(lf)* animals.
The data in B, D, E, F, and G are represented as mean ± SEM. ns = not significant and *p<0.05.

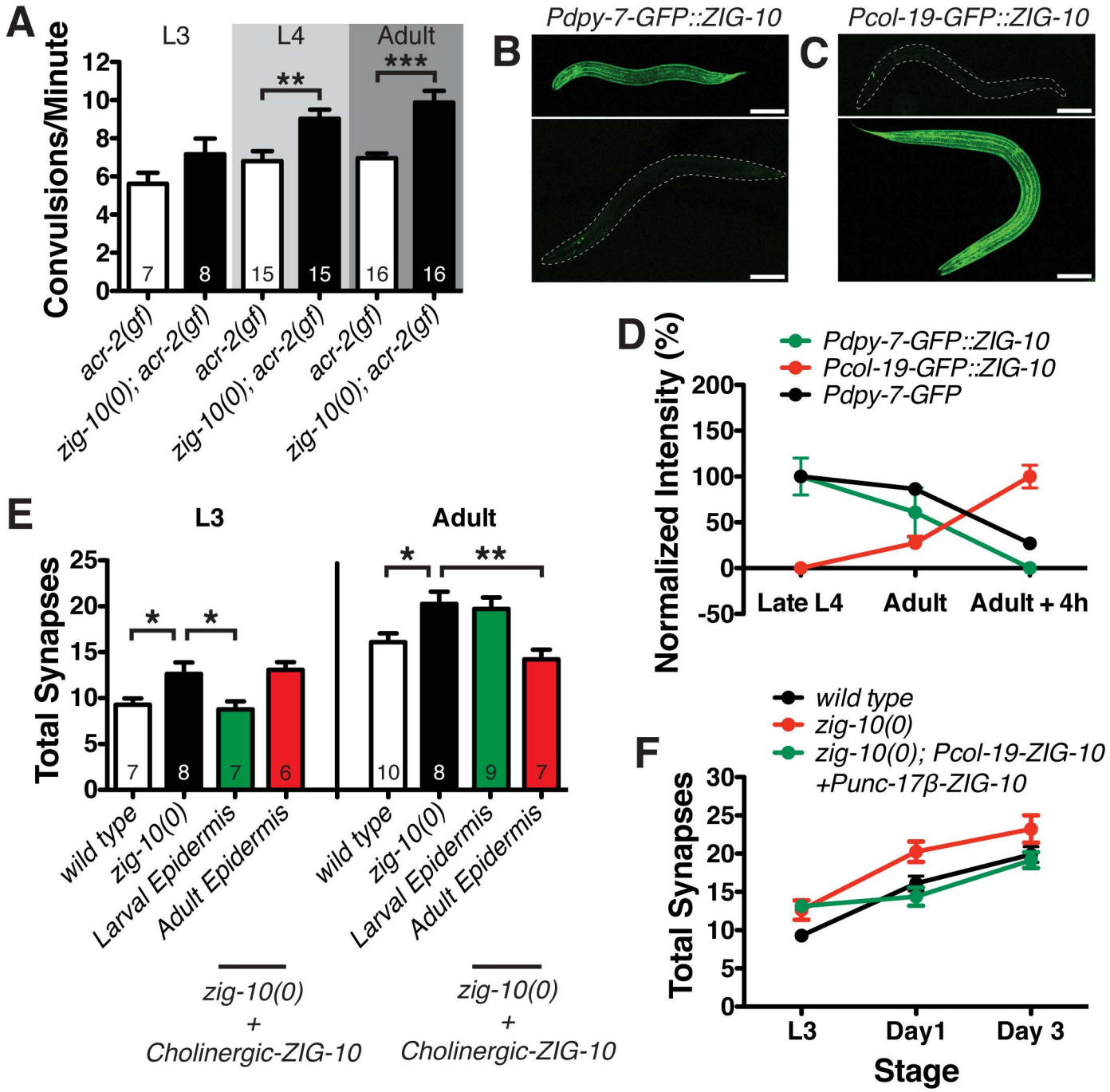

Figure S5, Related to Figure 5. Stage-Specific Regulation of Convulsion Frequency and Synapse Density.

(A) Loss of function in *zig-10* increased convulsion frequency of *acr-2(gf)* in larval and adult stages.
(B) Representative image of an L4 animal (top panel) and an adult (bottom panel) expressing *Pdpy-7-GFP::ZIG-10 (juEx5704)*.
(C) Representative image of an L4 animal (top panel) and an adult (bottom panel) expressing *Pcol-19-GFP::ZIG-10 (juEx5775)*.
(D) Time-course of GFP or GFP::ZIG-10 intensities from transgenes driven by the *dpy-7* or *col-19* promoters; *Pcol-19-GFP::ZIG-10* is visible until Day 3 or later (not shown).
(E) ZIG-10 is continuously required during development and adult stages to maintain cholinergic synapse density (visualized by *Pmig-13-CFP::RAB-3 (wyIs109)* in DA9 neurons).ZIG-10 was expressed under *Pdpy-7* (larval epidermis), *Pcol-19* (adult epidermis), and *Punc-17β* (cholinergic neurons).
(F) Quantification of cholinergic synapses (*wyIs109*) in L3, adult day 1 (Day 1), and adult day 3 (Day 3) animals.
The data in A, D, E, and F are represented as mean ± SEM. *p<0.05, **p≤0.01, and ***p≤0.001.

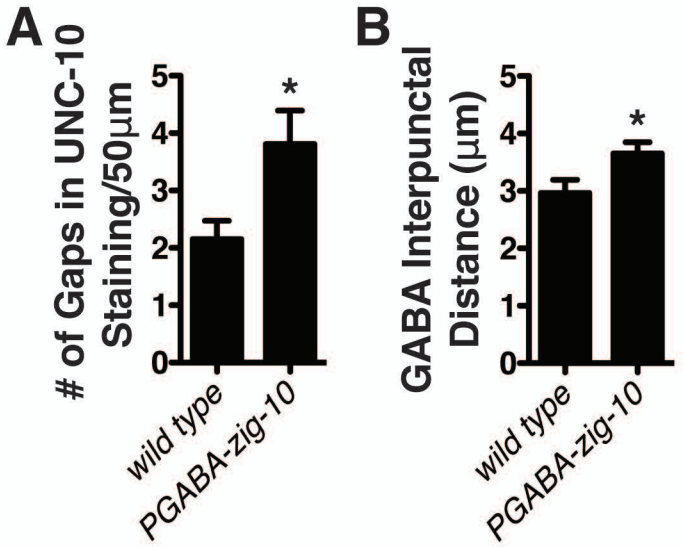

Figure S6, Related to Figure 6. Ectopic ZIG-10 increases gaps in UNC-10 staining and interpunctal distance between GABAergic synapses.

(A) GABAergic expression of ZIG-10 (*juEx7267*) showed an increase in the number of UNC-10 negative gaps.
(B) GABAergic expression of ZIG-10 (*juEx7267*) showed an increase in distance between GABAergic synapses labeled by SNB-1::GFP expressed under the *unc-25* promoter (*juIs1*).
Data are represented as mean ± SEM. *$p<0.05$.

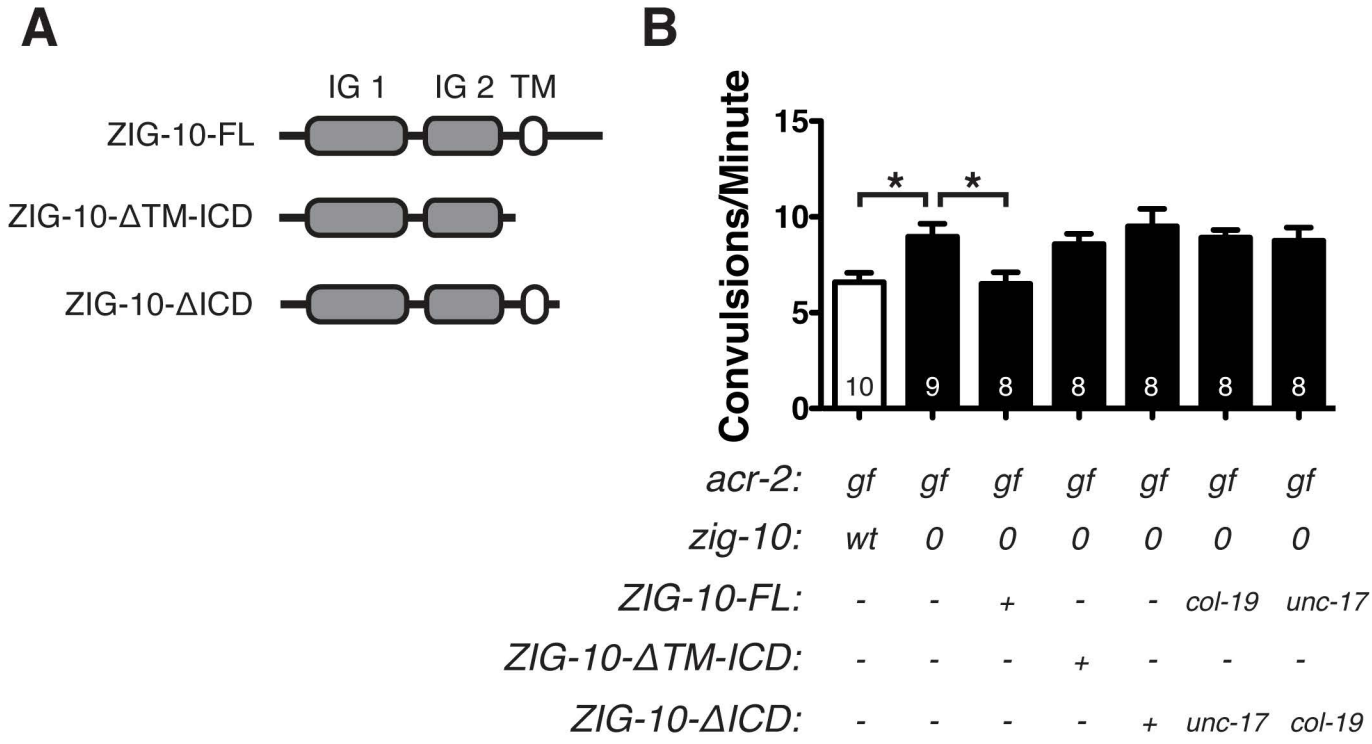

Figure S7, Related to Figure 7. The Transmembrane and Intracellular Domains are Required for ZIG-10 Function.

(A) Diagram of predicted proteins encoded by ZIG-10-FL, ZIG-10-ΔTM-ICD, and ZIG-10-ΔICD.
(B) Full-length ZIG-10 was required to reduce convulsion frequency in *zig-10(0); acr-2(gf)* animals. When coexpressing ZIG-10 full length (*juEx5775, juEx5706, or juEx5707*) and ZIG-10-ΔICD (*juEx6556, juEx6557, or juEx6558*), each transgene was injected separately then mated to produce multiple independent double transgenic lines that were analyzed. See Table S2.
Data in B are represented as mean ± SEM. *$p<0.05$.

Table S1, Related to Figure 1: Cell-adhesion related molecules screened by RNAi.

Gene	Clone ID/Allele	Convulsion frequency compared to vector
C27B7.7	IV-4F15	increase[a]
dig-1	III-3H03	no change
igcm-3	X-1P12	no change
ncam-1	X-1I17	no change
oig-4	II-5B02	no change
rig-3	X-3J19	no change
rig-6	II-4C15	no change[a]
sax-3	X-2C06	no change
sax-7	IV-4G03	no change
syg-1	X-1L16	no change
syg-2	X-6F16	no change
T04A11.3/C25G4.10	IV-6L09	no change
unc-40	I-2J21	no change
ZC374.2	X-4P02	no change
zig-1	I-4N08	no change
zig-10	II-5A05	increase
zig-2	X-5L12	no change
zig-3	X-4G13	no change
zig-4	X-4G09	no change
zig-5	III-5F18	no change
zig-6	X-2P22	no change
zig-7	I-2K03	no change
zig-8	III-6F01	no change

juIs345[Pcol-10-RDE-1]; rde-1(ne219); acr-2(n2420) (CZ16323) animals were synchronized, and L1 larvae were placed on plates containing HT115 bacteria expressing RNAi. 72 hours after plating, adult animals were assayed for convulsion frequency. [a] Genetic mutations did not recapitulate RNAi effect.

Table S3, Related to Figure 2: Plasmids created for this study.

Plasmid #	Plasmid Name	Promoter	3'UTR
pCZGY2615	*Pzig-10-GFP*	4.3kb sequence upstream of *zig-10* ATG	*unc-54*
pCZGY2602	*Pzig-10-GFP::ZIG-10*	4.3kb sequence upstream of *zig-10* ATG	*zig-10*
pCZGY2608	*Punc-17β-GFP::ZIG-10*	496bp sequence upstream of *unc-17* ATG	*zig-10*
pCZGY2607	*Pcol-19-GFP::ZIG-10*	665bp sequence upstream of *col-19* ATG	*zig-10*
pCZGY2606	*Pdpy-7-GFP::ZIG-10*	305bp sequence upstream of *dpy-7* ATG	*zig-10*
pCZGY2609	*Pmyo-3-GFP::ZIG-10*	2388bp sequence upstream of *myo-3* ATG	*zig-10*
pCZGY2617	*Punc-25-GFP::ZIG-10*	1254bp sequence upstream of *unc-25* ATG	*zig-10*
pCZGY2614	*Pzig-10-ZIG-10-ΔTM-ICD cDNA*	4.3kb sequence upstream of *zig-10* ATG	*unc-54*
pCZGY2613	*Pzig-10-ZIG-10b cDNA*	4.3kb sequence upstream of *zig-10* ATG	*unc-54*
pCZGY2619	*Pzig-10-ZIG-10-ΔICD cDNA*	4.3kb sequence upstream of *zig-10* ATG	*unc-54*
pCZGY2622	*Pcol-19-ZIG-10b cDNA*	665bp sequence upstream of *col-19* ATG	*unc-54*
pCZGY2621	*Punc-17β-ZIG-10b cDNA*	496bp sequence upstream of *unc-17* ATG	*unc-54*
pCZGY2624	*Pcol-19-ZIG-10-ΔICD cDNA*	665bp sequence upstream of *col-19* ATG	*unc-54*
pCZGY2623	*Punc-17β-ZIG-10-ΔICD cDNA*	496bp sequence upstream of *unc-17* ATG	*unc-54*
pCZ885	*Pcol-10-CED-1(Y1019F)::GFP*	1132bp sequence upstream of *col-10* ATG	*unc-54*
pCZ896	*Punc-17β-CED-1::GFP*	496bp sequence upstream of *unc-17* ATG	*unc-54*
pCZGY2756	*pcDNA 3.1-HA::ZIG-10*	CMV	*none*
pCZGY2759	*pcDNA 3.1-GFP::ZIG-10*	CMV	*none*
pCZGY2761	*pcDNA 3.1-HA::SRC-2*	CMV	*none*

Plasmids were created either using standard subcloning techniques using restriction enzymes or using the Gibson cloning method. LR reactions were performed between compatible Gateway plasmids (promoter destination vectors and entry vectors containing GFP, ZIG-10, or SRC-2) to obtain constructs for heterologous expression.

Table S4, Related to Figure 7: SH3-ligand motif containing genes screened by RNAi.

Gene	Clone ID	Convulsion frequency compared to vector
abl-1	X-5K23	no change
amph-1	IV-5A11	no change
ape-1	V-7N04	no change
C26C6.8	I-3B04	no change
C36E8.4	III-2A13	no change
C46H3.2	X-1G14	weak decrease
ccb-1	I-1D21	weak decrease
ccb-2	I-1K18	no change
ced-2	IV-8D15	weak decrease
ced-5	IV-5F11	weak decrease
ephx-1	II-3L15	no change
eps-8	IV-7L05	decrease
erp-1	X-2M14	no change
F19C7.8	IV-2I20	weak decrease
F42H10.3	III-4D17	no change
F49E2.2	X-4D02	no change
hum-1	I-4K18	no change
hum-4	X-5B15	no change
itsn-1	IV-8I23	no change
jip-1	II-1H04	no change
K08E3.4	III-6H08	no change
lin-2	X-5N10	no change
lst-4	IV-7I22	no change
magu-1	III-7G02	weak decrease
magu-2	V-6C10	weak decrease
magu-3	I-1N13	no change
magu-4	IV-5O13	no change
mlk-1	V-4E01	no change
nck-1	X-2F03	weak decrease
nphp-1	II-7O02	no change
plc-3	II-7O15	no change
prx-13	II-5D17	no change
rrc-1	X-4H20	no change
sdpn-1	X-4I09	no change
sem-5	X-4G19	no change
sma-1	V-8C09	no change
spc-1	X-2I13	weak decrease
src-2	I-7M09	decrease
stam-1	I-2B14	no change
T04C9.1	III-3K17	weak decrease
T04F8.7	X-5H07	no change
tbc-18	X-4E06	no change
toca-1	X-1B09	no change
toca-2	III-6H06	no change
unc-73	I-1B16	no change
unc-89	I-1B22	no change
vab-10	I-5L18	no change
vav-1	X-4L07	no change
W03A5.1	III-2H10	no change
Y106G6H.14	I-5A20	no change
Y44E3A.4	I-1B05	no change

Y47G6A.5	I-7N21	no change

zig-10(tm6127); acr-2(n2420); juEx6249 [Punc-25-GFP::ZIG-10+Pcol-19-GFP::ZIG-10] (CZ20628) adults were placed on HT115 bacteria expressing RNAi. 72 hours later the transgenic adult progeny were assayed for convulsion frequency.

Supplemental Experimental Procedures

Whole mount immunocytochemistry

One-day-old adult animals were collected with M9 solution, pelleted by centrifugation, and further washed with M9 and water. 1% paraformaldehyde in phosphate buffered saline (PBS, pH 7.4) was added to the worm pellet and freeze-thawed twice using liquid nitrogen. Worms were then frozen overnight at -80°C. Worms were then rapidly thawed and incubated at 4°C in cold room for 20 minutes. After washing three times with PBST (1% Triton X-100 in PBS) and one time in TTE (1% Triton X-100, 100 mM Tris-HCl, 1 mM EDTA), the cuticle was permeabilized by incubating in 1% beta-mercaptoethanol in TTE for 4 hours at 37°C on a rotator. Following a wash with borate buffer (1% Triton X-100, 20 mM H_3BO_3, 10 mM NaOH, pH 9.3) the worms were incubated in 10 mM DTT in borate buffer for 15 minutes at 37 °C on a rotator. After washing with borate buffer, the worms were then incubated in 0.3 % H_2O_2 in borate buffer at room temperature on a rotator. The worms were then washed in PBST three times and were incubated with 5% goat serum in PBST for 1 hour at room temperature on a rotator. The worms were then incubated with mouse anti-UNC-10/RIM2 (1:50, RRID:AB_10570332, Developmental Studies Hybridoma Bank, IA), or anti-GFP (1:500, A1112, RRID:AB_10073917, Invitrogen, CA) in 5% goat serum in PBST overnight at 4°C on a shaker. After washing three times in PBST, the worms were incubated with a secondary antibody against mouse (1:2000 anti-mouse Alexa 594, RRID:AB_141372, or anti-rabbit Alexa 488, RRID: AB_143165, Invitrogen, CA) in 5% goat serum in PBST for 1 hour at room temperature. Following three washes with PBST, the worms were mounted on a glass slide with Vectashield mounting media (RRID: AB_2336789, Vector Labs, CA).

Electron Microscopy Analysis of Synapses

Electron microscopy sections were prepared as previously described (Kittelmann et al., 2013). About 1200 serial sections were collected for wild type and *zig-10(0)* animals, and ~30-50 synapses were analyzed for active zone length and ~100-200 synapses were analyzed for docked synaptic vesicles. We observed no differences between wild type and *zig-10(0)* in either active zone length or docked vesicles in cholinergic neurons.

Supplemental References

Babu, K., Hu, Z., Chien, S.C., Garriga, G., and Kaplan, J.M. (2011). The immunoglobulin super family protein RIG-3 prevents synaptic potentiation and regulates Wnt signaling. Neuron. *71*, 103-116.

Ch'ng, Q., Sieburth, D., and Kaplan, J.M. (2008). Profiling synaptic proteins identifies regulators of insulin secretion and lifespan. PLoS Genet. *4*, e1000283.

Gendrel, M., Rapti, G., Richmond, J.E., and Bessereau, J.L. (2009). A secreted complement-control-related protein ensures acetylcholine receptor clustering. Nature. *461*, 992-996.

Hallam, S.J., and Jin, Y. (1998). lin-14 regulates the timing of synaptic remodelling in Caenorhabditis elegans. Nature. *395*, 78-82.

Jensen, M., Hoerndli, F.J., Brockie, P.J., Wang, R., Johnson, E., Maxfield, D., Francis, M.M., Madsen, D.M., and Maricq, A.V. (2012). Wnt signaling regulates acetylcholine receptor translocation and synaptic plasticity in the adult nervous system. Cell. *149*, 173-187.

Jospin, M., Qi, Y.B., Stawicki, T.M., Boulin, T., Schuske, K.R., Horvitz, H.R., Bessereau, J.L., Jorgensen, E.M., and Jin, Y. (2009). A neuronal acetylcholine receptor regulates the balance of muscle excitation and inhibition in *Caenorhabditis elegans*. PLoS Biol. *7*, e1000265.

Kinchen, J.M., Cabello, J., Klingele, D., Wong, K., Feichtinger, R., Schnabel, H., Schnabel, R., and Hengartner, M.O. (2005). Two pathways converge at CED-10 to mediate actin rearrangement and corpse removal in C. elegans. Nature. *434*, 93-99.

Kittelmann, M., Hegermann, J., Goncharov, A., Taru, H., Ellisman, M.H., Richmond, J.E., Jin, Y., and Eimer, S. (2013). Liprin-alpha/SYD-2 determines the size of dense projections in presynaptic active zones in C. elegans. J Cell Biol. *203*, 849-863.

Martin, J.A., Hu, Z., Fenz, K.M., Fernandez, J., and Dittman, J.S. (2011). Complexin has opposite effects on two modes of synaptic vesicle fusion. Curr Biol. *21*, 97-105.

Poon, V.Y., Klassen, M.P., and Shen, K. (2008). UNC-6/netrin and its receptor UNC-5 locally exclude presynaptic components from dendrites. Nature. *455*, 669-673.

Richmond, J.E., Davis, W.S., and Jorgensen, E.M. (1999). UNC-13 is required for synaptic vesicle fusion in C. elegans. Nat Neurosci. *2*, 959-964.

Sakaguchi-Nakashima, A., Meir, J.Y., Jin, Y., Matsumoto, K., and Hisamoto, N. (2007). LRK-1, a *C. elegans* PARK8-related kinase, regulates axonal-dendritic polarity of SV proteins. Curr Biol. *17*, 592-598.

Venegas, V., and Zhou, Z. (2007). Two alternative mechanisms that regulate the presentation of apoptotic cell engulfment signal in Caenorhabditis elegans. Mol Biol Cell. *18*, 3180-3192.

Xu, S., and Chisholm, A.D. (2011). A Galphaq-Ca(2)(+) signaling pathway promotes actin-mediated epidermal wound closure in *C. elegans*. Curr Biol. *21*, 1960-1967.

Zhou, Z., Hartwieg, E., and Horvitz, H.R. (2001). CED-1 is a transmembrane receptor that mediates cell corpse engulfment in *C. elegans*. Cell. *104*, 43-56.